RSC Advances

ROYAL SOCIETY OF CHEMISTRY

www.rsc.org/advances

RSC Advances

COMMUNICATION

Spray Reaction Prepared $FA_{1-x}Cs_xPbI_3$ Solid Solution as Light Harvester for Perovskite Solar Cells with Improved Humidity Stability

Received 00th January 20xx,
Accepted 00th January 20xx

DOI: 10.1039/x0xx00000x

www.rsc.org/

Xiang Xia,[a] Wenyi Wu,[b] Hongcui Li,[a] Bo Zheng,[a] Yebin Xue,[a] Jing Xu,[a] Dawei Zhang,[a] Chunxiao Gao[b] and Xizhe Liu*[a]

$FA_{1-x}Cs_xPbI_3$ solid solution films are prepared as light harvester for perovskite solar cells by spray reaction. Cs^+ ions can improve the quality of light harvester film, and the average PCE of devices increases from 11.3% for $FAPbI_3$ to 14.2% for $FA_{0.9}Cs_{0.1}PbI_3$. Moreover, $FA_{0.9}Cs_{0.1}PbI_3$-based devices exhibit remarkable improvement on humidity stability.

Inorganic-organic lead halide is a kind of solution processable semiconductor with excellent photovoltaic performance.[1–2] This kind of materials has a perovskite structure of AMX_3, and small organic ammonium cations occupy the A sites (M represents lead and X represents halogen). Methylammonium ($CH_3NH_3^+$, MA^+) is a wildly used organic ammonium cation in this material. Since the previous reports define the basic structure of perovskite solar cells,[3–4] the devices based on perovskite materials with MA^+ ions have been extensively investigated[5–14] and their best power conversion efficiency (PCE) reaches about 20% under one sun condition.[15,16]

This kind of perovskite materials can also employ an alternative organic ammonium cation of formamidinium ($HC(NH_2)_2^+$, FA^+), which is promising for broadening the wavelength range of light absorption.[17–29] And it is noted that the band gap of $FAPbI_3$ (1.48 eV) is closer to the ideal band gap of solar cells than that of $MAPbI_3$ (1.57 eV).[27,28] However, the devices based on pure $FAPbI_3$ usually have lower PCE than the devices based on $MAPbI_3$.[27,30,31] Although the α-phase $FAPbI_3$ is the desirable material for photovoltaic application, the δ-phase $FAPbI_3$, which seriously damages the performance of the device, emerges easily in the preparation process.[27] Thermal treatment is necessary for translating the δ-phase $FAPbI_3$ into its α-phase, but thermal decomposition usually arises at the elevated temperature.[18,32] These factors lead to the difficulty for fabricating $FAPbI_3$ films with high quality. Moreover, α-phase $FAPbI_3$ easily translates into δ-phase at room temperature in the wet air condition, which sincerely decreases the stability of perovskite solar cells.[27] Therefore, the simultaneous improvement on both the quality and the humidity stability of perovskite films becomes desirable.

The solid solution of perovskite materials usually preserves the photovoltaic property, while the detailed physical properties can be adjusted. Several works about solid solutions of perovskite materials are reported, where MA^+ ions can be partially replaced by FA^+ or cesium (Cs^+) ions and I^- ions can be partially replaced by Br^- or Cl^- ions.[30–37] It is found that the doping atoms can affect the photovoltaic performance of the corresponding devices remarkably. Recently, it is also reported that the quality of α-phase $FAPbI_3$ films can be improved by the formation of solid solutions, such as $FA_{1-x}MA_xPbI_{3-x}Br_x$ and $FA_{1-x}MA_xPbI_3$.[32,38] As a consequence, highly efficient perovskite solar cells based on $FA_{1-x}MA_xPbI_{3-x}Br_x$ is produced by the intramolecular exchange method, and the best PCE of 20.2% is achieved.[39] To form the perovskite structure of AMX_3, organic ammonium cations must fit the space composed of four adjacent corner sharing MX_6 octahedra. The relatively large size of FA^+ ions leads to the extension of PbI_6 octahedra matrices in $FAPbI_3$. Solid solution can be a method for relaxing the PbI_6 matrices by partially replacing large FA^+ ion with small Cs^+ ion, which can also occupy the A site in several perovskite materials with AMX_3 structure.[40,41]

Spray technique is a wildly used method in industry process, and it is also an enlargeable technique for preparing perovskite light harvester films.[42] In the preparation of $FA_{1-x}Cs_xPbI_3$ solid solution, conventional solution based method has the possibility of phase separation in the process of solvent evaporation. For the spray reaction, most solvent converts to vapor before arriving at the iodide surface. Therefore, spray reaction method is likely to facilitate the formation of $FA_{1-x}Cs_xPbI_3$ solid solution films with pure phase structure.

[a] Institute of Atomic and Molecular Physics, Jilin Provincial Key Laboratory of Applied Atomic and Molecular Spectroscopy, Jilin University, Changchun, 130012, China, E-mail: liu_xizhe@jlu.edu.cn
[b] State Key Laboratory for Superhard Materials, Jilin University, Changchun, 130012, China

† Footnotes relating to the title and/or authors should appear here.
Electronic Supplementary Information (ESI) available: Experimental details. See DOI: 10.1039/x0xx00000x

In this study, we prepare a series of $FA_{1-x}Cs_xPbI_3$ light harvester films by an interface reaction method based on the spray technique. The crystal structure and light absorption of these light harvester films are characterized, and the solar cells with these films are investigated. Pure α-phase structure can be obtained for the Cs^+ incorporation range up to 30%, which permits us to give a systematic investigation on this solid solution material.

Firstly, the fluorine doped tin oxide (FTO) glass substrate was etched and cleaned. 30 nm compact TiO_2 film and 200 nm mesoporous TiO_2 film were sequentially deposited by spray pyrolysis and spin-coating. Then $FA_{1-x}Cs_xPbI_3$ perovskite film was prepared on the TiO_2 film by an interface reaction method based on the spray technique. Certain amounts of CsI were added in 462 mg/mL PbI_2 N,N-Dimethylformamide (DMF) solution following the Cs/Pb ratio of $FA_{1-x}Cs_xPbI_3$ (x=0, 0.1, 0.2 and 0.3). This CsI/PbI_2 mixed solution or pure PbI_2 solution were spin-coated on the mesoporous TiO_2 film. After preheating at the reaction temperature for 5 min, 50 mg/mL FAI in isopropanol solution was sprayed on the top of the PbI_2 film at 160 ^oC for the interface reaction. Finally, the perovskite film was washed with isopropanol and annealed at the reaction temperature for 10 min. $FA_{1-x}Cs_xPbI_3$ films were also prepared at different reaction temperatures, the x-ray diffraction (XRD) and scanning electron microscopy (SEM) analyses were shown in the supporting information (Fig. S1 and S2). To fabricate perovskite solar cell, a hole-conductor layer and a gold top electrode were deposited on the $FA_{1-x}Cs_xPbI_3$ perovskite film sequentially by spin-coating and thermal evaporation. The cross-sectional morphology of a perovskite solar cell is shown in Fig. S3. Experimental detail is provided in the supporting information.

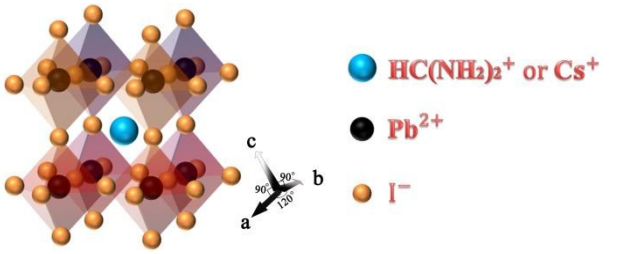

Scheme 1 Schematic illustration of the crystal structure of $FAPbI_3$ with Cs^+ ions incorporation.

Schematic illustration of the crystal structure of $FAPbI_3$ with Cs^+ ions incorporation is shown in Scheme 1. Four kinds of $FA_{1-x}Cs_xPbI_3$ films (x=0, 0.1, 0.2 and 0.3) are prepared, and the amounts of Cs^+ in the films are confirmed by energy dispersive x-ray spectroscopy (EDS) measurement (Table S1) and x-ray photoelectron spectroscopy (XPS) measurement (Fig. S5 and

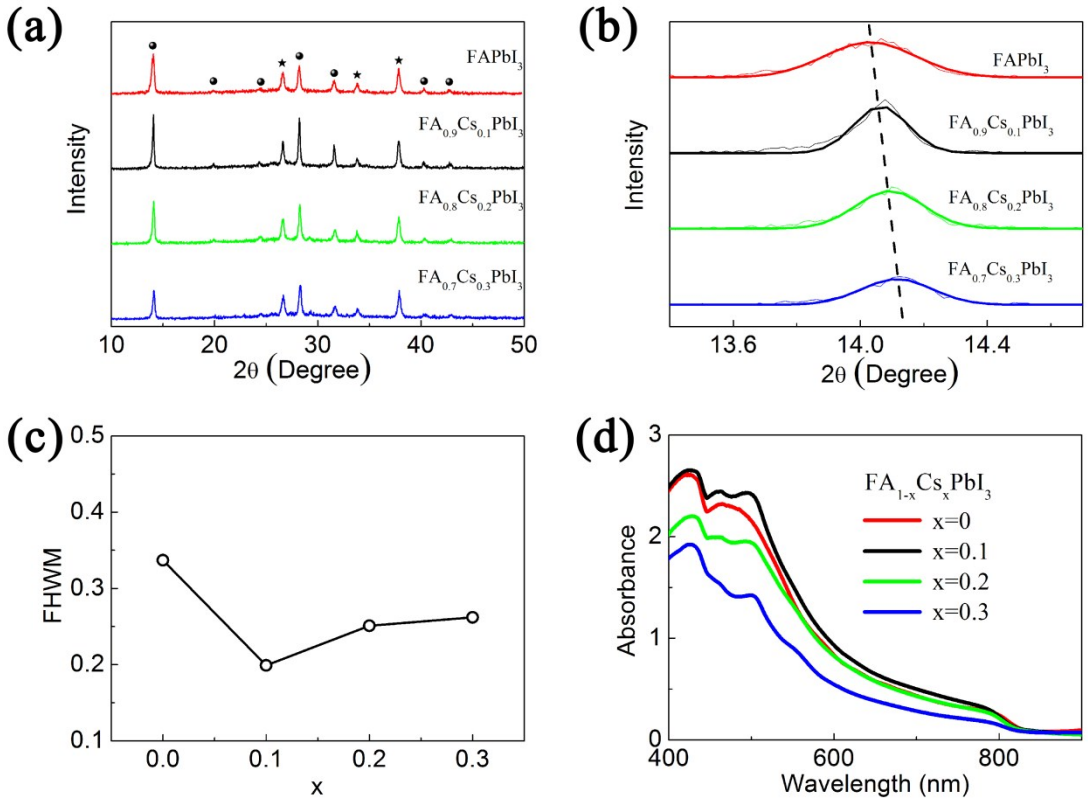

Fig. 1 (a) XRD patterns of $FA_{1-x}Cs_xPbI_3$ (x=0, 0.1, 0.2 and 0.3) films. The XRD peaks assigned to perovskite and FTO substrate are marked with solid circles and asterisks, respectively. (b) (110) diffraction peaks of $FA_{1-x}Cs_xPbI_3$ films. (c) Full width of half maximum (FWHM) of the (110) diffraction peaks. (d) Absorption spectra of $FA_{1-x}Cs_xPbI_3$ films.

Table S2). Fig. 1(a) is the XRD patterns of these four $FA_{1-x}Cs_xPbI_3$ films with different Cs^+ concentrations. Except three diffraction peaks from the substrate, all diffraction peaks can be assigned to the trigonal crystal structure of $FAPbI_3$ film. It means that our spray reaction method can produce pure α-phase $FAPbI_3$ films at the optimized reaction condition. In Fig. 1(a), the incorporation of Cs^+ ions in the $FAPbI_3$ films does not change the XRD patterns of pure α-phase structure. It means that spray reaction method avoids phase separation in the formation of these solid solution films. Fig. 1(b) shows the (110) diffraction peaks of four $FA_{1-x}Cs_xPbI_3$ films with different Cs^+ concentrations. The 2θ angle of diffraction peak increases with the increase of Cs^+ concentration. We calculate the lattice parameters of $FA_{1-x}Cs_xPbI_3$ by the corresponding XRD patterns, which are summarized in Table S3. It indicates the lattice constant can be modified by controlling the concentration of Cs^+ ions, and the more Cs^+ ions incorporate the smaller the lattice constant is. This relationship implies that Cs^+ ions replace FA^+ ions by occupying the A site of AMX_3 structure than the interstitial site. And the substitutional solid solution of $FA_{1-x}Cs_xPbI_3$ can be produced in the Cs^+ concentration up to 30% by the spray reaction method. The decrease of lattice constant in the $FA_{1-x}Cs_xPbI_3$ films is related to relax the extension in the PbI_6 matrices. Furthermore, the full width of half maximum (FWHM) of the (110) diffraction peaks in these four films are also different, which is summarized in Fig. 1(c). The FWHM of $FAPbI_3$ film (0.337^o) is much larger than that of $FA_{0.9}Cs_{0.1}PbI_3$ (0.199^o), while the FWHMs are 0.251^o and 0.262^o for $FA_{0.8}Cs_{0.2}PbI_3$ and $FA_{0.7}Cs_{0.3}PbI_3$, respectively. The broadening of XRD peaks are usually induced by the low quality of crystallization in the films. Then the smallest FWHM of $FA_{0.9}Cs_{0.1}PbI_3$ film reflects its highest quality among these four kinds of films. The incorporation of Cs^+ ions also induces the variation of light absorption as show in Fig. 1(d). The absorption edge blue shifts by increasing Cs^+ concentration. The energy band gaps of $FA_{1-x}Cs_xPbI_3$ films are calculated by the absorption edge according to Kubellka-Munk equation, which are summarized in Fig. S6 and Table S4. It indicates Cs^+ ions incorporation increases the band gap of $FA_{1-x}Cs_xPbI_3$. It is noted that light absorption intensity is also different for $FA_{1-x}Cs_xPbI_3$ films with different Cs^+ concentrations. Although large Cs^+ concentration ($FA_{0.7}Cs_{0.3}PbI_3$) induces remarkable decrease in the absorption intensity, $FA_{1-x}Cs_xPbI_3$ with small Cs^+ concentration ($FA_{0.9}Cs_{0.1}PbI_3$) exhibits higher absorption intensity than $FAPbI_3$ in the wavelength range of 400~800 nm.

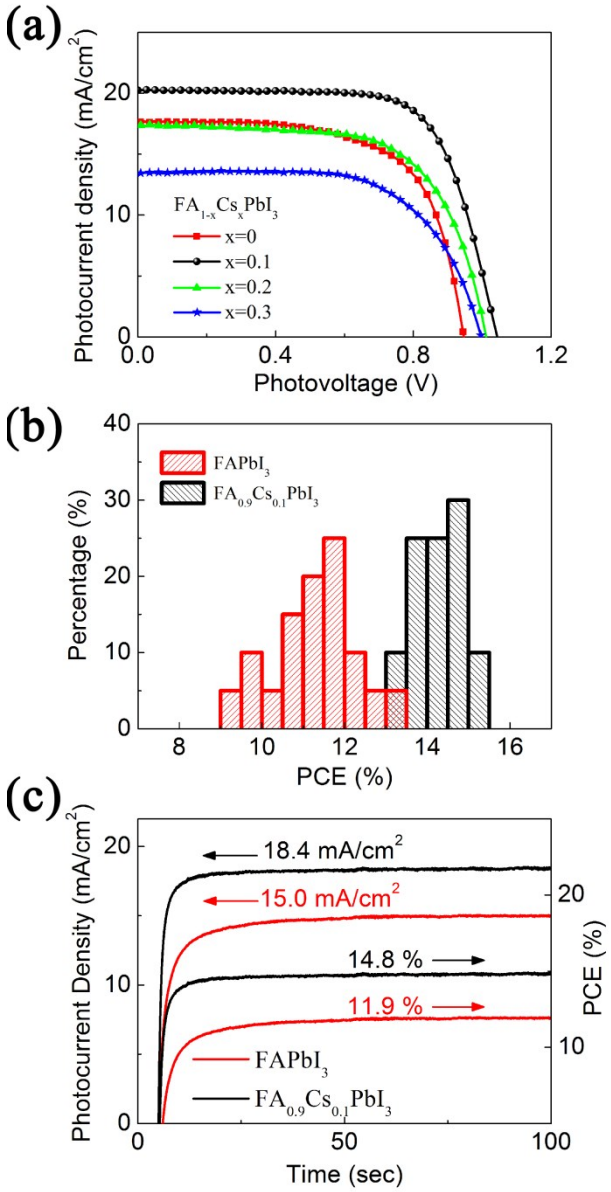

Fig. 2 (a) Photocurrent density-photovoltage characteristics of the $FA_{1-x}Cs_xPbI_3$-based devices (x=0, 0.1, 0.2 and 0.3). (b) Statistics of efficiencies for both $FAPbI_3$-based and $FA_{0.9}Cs_{0.1}PbI_3$-based devices. (c) Photocurrent density and PCE as a function of light soaking time measured at maximum power point (0.793 V for $FAPbI_3$-based devices and 0.804 V for $FA_{0.9}Cs_{0.1}PbI_3$-based device).

We fabricate perovskite solar cells based on these four kinds of $FA_{1-x}Cs_xPbI_3$ materials. The photocurrent density-photovoltage characteristics of corresponding devices are shown in Fig. 2(a), and the photovoltaic parameters are summarized in Table 1. By the Cs^+ ion incorporation, the short circuit current density (J_{SC}) of corresponding devices increases from 17.7 mA/cm^2 at x=0 to 20.3 mA/cm^2 at x=0.1, whereas further increasing the amount of Cs^+ ions decreases J_{SC} to 17.4 mA/cm^2 at x=0.2 and 13.4 mA/cm^2 at x=0.3. Moreover, the

Table 1 The photovoltaic parameters of the devices based on $FA_{1-x}Cs_xPbI_3$ (x=0, 0.1, 0.2 and 0.3).

$FA_{1-x}Cs_xPbI_3$	Jsc (mA/cm^2)	Voc (V)	Fill factor	PCE (%)
x=0	17.7	0.95	0.65	11.0
x=0.1	20.3	1.05	0.70	14.9
x=0.2	17.4	1.01	0.67	11.8
x=0.3	13.4	0.99	0.66	8.7

open circuit voltage (V_{OC}) is also increased from 0.95 V at x=0 to 1.05 V at x=0.1, and then decrease to 1.01 V at x=0.2 and 0.99 V at x=0.3. As a result, the PCE of corresponding devices is enhanced from 11.0% to 14.9% by replacing 10% FA^+ ions of $FAPbI_3$ with Cs^+ ions. The statistics comparison between PCEs of both $FAPbI_3$-based and $FA_{0.9}Cs_{0.1}PbI_3$-based devices is shown in Fig. 2(b). $FA_{0.9}Cs_{0.1}PbI_3$-based devices show an average efficiency of 14.2% with narrow distribution range, which is obviously better than that of $FAPbI_3$-based devices (11.3%). This result indicates that Cs^+ ion incorporation can improve the performance of perovskite solar cells based on $FAPbI_3$. We measure the variation of current density with the light soaking time at the constant bias voltage of maximum power condition (V_{opt} is about 0.8 V). As shown in Fig. 2(c), both $FAPbI_3$-based and $FA_{0.9}Cs_{0.1}PbI_3$-based devices exhibit stabilized power conversion efficiency after 100 seconds light soaking, but the transient time is different. $FA_{0.9}Cs_{0.1}PbI_3$-based device reaches 90% of its stabilized PCE in 3.4 seconds, while $FAPbI_3$-based device needs 8.5 seconds for this transient process. It implies that Cs^+ ions incorporation can accelerate to establish the balance state in the devices.

Fig. 3(a) is the incident photon-to-electron conversion efficiency (IPCE) spectra of devices based on $FA_{1-x}Cs_xPbI_3$ films. At short wavelength range (below 500 nm), all devices based on these four $FA_{1-x}Cs_xPbI_3$ films exhibit good IPCE values. This can be related to the large absorption coefficient of $FA_{1-x}Cs_xPbI_3$ films at the short wavelength range. For devices based on $FAPbI_3$, the onset wavelength of IPCE is at 850 nm. After the incorporation of Cs^+ ions, the onset wavelength blue shifts to 841 nm, this is in accordance with the blue shifting of absorption edge. It is noted that the onset wavelength of devices based on $FA_{0.9}Cs_{0.1}PbI_3$ films is still obviously longer than that of devices based on $MAPbI_3$ films (at about 800 nm)[32]. At the middle wavelength range (600 to 700 nm), the IPCE spectra of devices based on these four $FA_{1-x}Cs_xPbI_3$ films have remarkable different IPCE values. The incorporation of 10% Cs^+ ions can increase the IPCE value of corresponding devices, while further increasing the concentration of Cs^+ ions leads to the decrease of IPCE value in the middle wavelength range. Although the trend of IPCE value is in accordance with the absorption spectra, the remarkable difference on IPCE values cannot be fully attributed to the minor difference of light absorption. SEM images of $FA_{1-x}Cs_xPbI_3$ with four different Cs^+ ion concentrations are shown in Fig. S7. Although these $FA_{1-x}Cs_xPbI_3$ films have similar morphology with compact structure, the grain sizes are different. The grain size distributions are analyzed by Nano Measurer software. The average grain size of $FA_{0.9}Cs_{0.1}PbI_3$ film is 257 nm, which is the largest one in these four samples. As previous reports[7,19], the perovskite film with large crystal grains has improved crystallization and

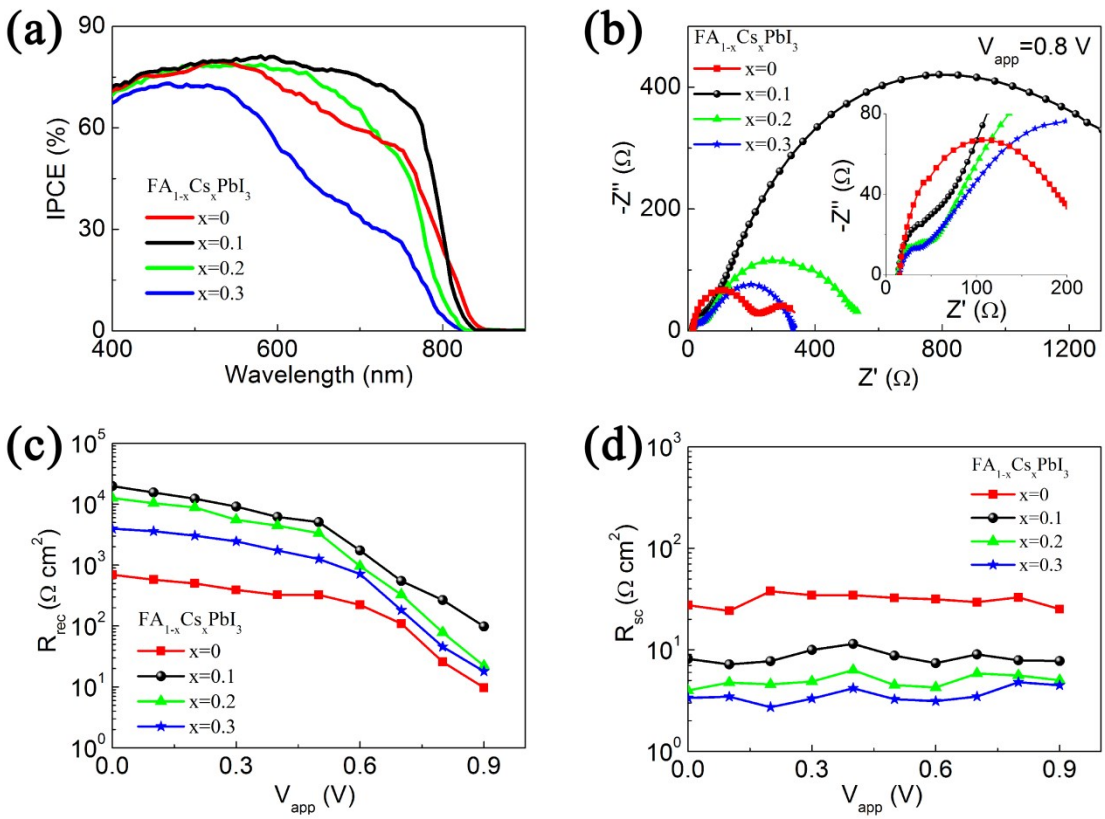

Fig. 3 (a) IPCE spectra of the $FA_{1-x}Cs_xPbI_3$-based devices (x=0, 0.1, 0.2 and 0.3). (b) Nyquist plots of $FA_{1-x}Cs_xPbI_3$-based devices measured at 0.8 V applied voltage. (c) Recombination resistance (R_{rec}) at different applied voltage. (d) Selective contact resistance (R_{sc}) at different applied voltage.

reduced crystal interfaces, which are beneficial to the recombination and transportation process. These improvements can increase the IPCE value of devices. The SEM analysis is accordance with the smallest FHWM of $FA_{0.9}Cs_{0.1}PbI_3$ film in the XRD measurement. We perform impedance spectroscopy (IS) experiments to investigate the recombination and transportation process.

Impedance spectroscopy of perovskite solar cells measured at 0.8 V applied voltage are shown in Fig. 3(b). The obtained impedance data can be fitted with the equivalent circuit (Fig. S8) to extract the impedance parameters, such as the recombination resistance in the perovskite layer (R_{rec}) and the charge transfer resistance at the interfaces of selective contacts (R_{sc}). As previous reports [43–45], the low frequency arc of the impedance spectra can be attributed to the recombination process, and the corresponding resistance (R_{rec}) is inversely related to the recombination rate of photo-generated electrons. The high frequency arc of the impedance spectra is influenced by the charge transfer resistance at the selective contact layer/perovskite interfaces, and also by the transport resistance in the selective contact layers [43,44]. As the selective contact layers do not change in this experiment, the observed differences of high frequency impedance can be attributed to the charge transfer process at the selective contact layer/perovskite interfaces.

R_{rec} obtained at different applied potentials are summarized in Fig. 3(c). The R_{rec} with large applied potential is inversely proportion to the recombination rate. It can be observed that the device based on $FAPbI_3$ exhibits the smallest R_{rec}. The fast recombination leads to the low carrier density, which is accordance with the low open circuit voltage (0.95 V) of the $FAPbI_3$-based device in Fig. 2(a). By incorporation of 10% Cs^+ ions in the $FAPbI_3$ films, R_{rec} increases remarkably and a V_{OC} of 1.05 V is obtained for the corresponding device. Further increasing the concentration of Cs^+ ions to 20% and 30%, the R_{rec} of corresponding devices reduce gradually, which is accordance with the decrease of V_{OC} in Fig. 2(a). The trend of recombination process is also accordance with the quality of crystallization in the corresponding $FA_{1-x}Cs_xPbI_3$ films in Fig. 1(c). It means that improving the quality of light harvester films is an effective way to decease the recombination rate in the perovskite solar cells.

Fig. 3(d) shows the R_{sc} obtained at different applied potentials. R_{sc} almost does not change at various applied potentials, and it decreases with the increase of Cs^+ concentration in $FA_{1-x}Cs_xPbI_3$. It implies that Cs^+ incorporation is beneficial for the charge transfer at the selective contact layer/perovskite interfaces. R_{sc} is related with the series resistance of solar cells, while R_{rec} at low applied voltage reflects the shunt resistance. Small R_{sc} and large R_{rec} lead to good fill factor of solar cells.[43] As a result, the fill factor of $FAPbI_3$-based device (0.65) is enhanced to 0.70 by the 10% incorporation of Cs^+ ions. Although $FA_{0.8}Cs_{0.2}PbI_3$-based and $FA_{0.7}Cs_{0.3}PbI_3$-based devices have lower R_{sc} than $FA_{0.9}Cs_{0.1}PbI_3$-based device, the decrease of R_{rec} at low applied voltage lead to the slightly decrease in fill factor (0.67 and 0.66).

Moreover, the stability of unsealed devices based on $FAPbI_3$ and $FA_{0.9}Cs_{0.1}PbI_3$ films are investigated in the environment of 50% humidity at 20 °C for 100 hours. The PCE decay is summarized in Fig. 4(a). In the first five hours, the PCE of device with $FAPbI_3$ light harvester film decreases from 11.4% to 3.58%. It further decreases to 0.35% after the aging of 100 hours. On the contrary, the PCE of device with $FA_{0.9}Cs_{0.1}PbI_3$ light harvester film decreases from 14.5% to 12.4% in the first five hours, and no obviously change is detected in the following time of 100 hours aging (12.5% at 100 hours). The photographs of these devices with and without aging process are shown in the supporting information (Fig. S9). After 100 hours aging, the $FAPbI_3$-based device becomes yellow in color, while the $FA_{0.9}Cs_{0.1}PbI_3$-based device remains its dark brown color. This result indicates 10% Cs^+ ions incorporation leads to remarkable improvement on the humidity stability of devices.

We also age naked $FAPbI_3$ and $FA_{0.9}Cs_{0.1}PbI_3$ films without hole conductor layers and Au electrode layers in the same condition. Fig. 4(b) shows the corresponding XRD patterns of these films before and after the aging process. Before humidity aging, both $FAPbI_3$ and $FA_{0.9}Cs_{0.1}PbI_3$ films give a set of strong peaks, which indicate an α-phase crystal structure of halide perovskite (marked with solid circles). After 100 hours aging, the peaks of δ-phase $FAPbI_3$ appear in the XRD patterns of the

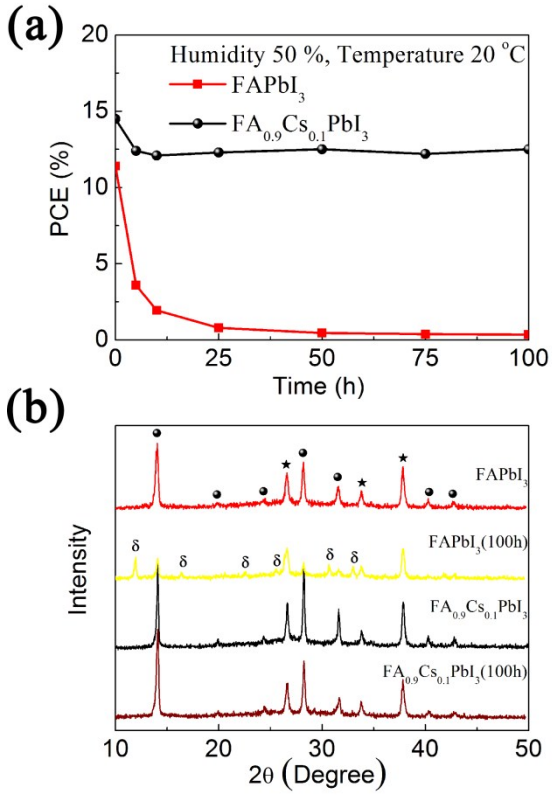

Fig. 4 (a) PCE of both $FAPbI_3$-based and $FA_{0.9}Cs_{0.1}PbI_3$-based devices (unsealed) with aging time in 50% humidity and 20 °C environment. (b) XRD patterns of $FAPbI_3$ film and $FA_{0.9}Cs_{0.1}PbI_3$ film before and after aging in 50% humidity and 20 °C environment for 100 h. The XRD peaks assigned to α-phase and δ-phase are marked with solid circles and δ, respectively.

$FAPbI_3$ film (marked with δ), and the peaks of α-phase $FAPbI_3$ greatly attenuate. It indicates that most of α-phase $FAPbI_3$ changes into δ-phase $FAPbI_3$ in the aging process. As δ-phase $FAPbI_3$ cannot act as an effective light harvester for perovskite solar cell, the remarkable performance decay of $FAPbI_3$-based device in Fig. 4(a) can be attributed to the damage of α-phase $FAPbI_3$ film. On the contrary, $FA_{0.9}Cs_{0.1}PbI_3$ film still shows strong diffraction peaks of α-phase after the aging process, and no peak for δ-phase is observed. The undamaged $FA_{0.9}Cs_{0.1}PbI_3$ light harvester film leads to the stable performance of device in the aging process. This result indicates the Cs^+ ions incorporation can enhance the stability of α-phase structure, which is the major factor for improving the humidity stability of perovskite photovoltaic devices.

Conclusions

In summary, we prepare a series of $FA_{1-x}Cs_xPbI_3$ solid solution films as the light harvester in perovskite solar cells by the spray reaction method. XRD analysis reflects that solid solution with pure α-phase structure is obtained in the Cs^+ concentration up to 30%, and its lattice constant can be adjusted by controlling Cs^+ concentration. By optimizing the composition of $FA_{1-x}Cs_xPbI_3$ films, the average PCE of devices is enhanced from 11.3% for $FAPbI_3$ to 14.2% for $FA_{0.9}Cs_{0.1}PbI_3$. This improvement can be attributed to the increase of light absorption intensity and the decrease of recombination process. Furthermore, $FA_{0.9}Cs_{0.1}PbI_3$ also exhibits better humidity stability than $FAPbI_3$. In the 50% humidity environment, α-phase $FAPbI_3$ rapidly translates into its δ-phase, and the PCE of $FAPbI_3$-based device decreases to 0.35% after the aging of 100 hours. On the contrary, $FA_{0.9}Cs_{0.1}PbI_3$ remains its α-phase structure in the humidity aging process, and the PCE of corresponding device keeps constant at about 12.5% after the initially minor decrease.

Acknowledgements

This work was partially supported by National Natural Science Foundation of China (Grant Nos. 51273079, 11374121), National Basic Research Program of China (Grant No. 2011CB808204), the Science Development Program of JiLin Province (Grant No. 20150519021JH), and the Fundamental Research Funds for Central Universities at Jilin University.

Notes and references

1 A. Kojima, K. Teshima, Y. Shirai and T. Miyasaka, *J. Am. Chem. Soc.,* 2009, **131**, 6050.
2 J. Im, C. Lee, J. Lee, S. Park and N. Park, *Nanoscale,* 2011, **3**, 4088.
3 H. Kim, C. Lee, J. Im, K. Lee, T. Moehl, A. Marchioro, S. Moon, R. Humphry-Baker, J. Yum, J. Moser and M. Grätzel, *Sci. Rep.,* 2012, **2**, 591.
4 M. Lee, J. Teuscher, T. Miyasaka, T. Murakami and H. Snaith, *Science,* 2012, **338**, 643.
5 M. Liu, M. Johnston and H. Snaith, *Nature* 2013, *501*, 395.
6 J. Burschka, N. Pellet, S. Moon, R. Humphry-Baker, P. Gao, M. Nazeeruddin and M. Grätzel, *Nature,* 2013, **499**, 316.
7 J. Im, I. Jang, N. Pellet, M. Grätzel and N. Park, *Nat. Nanotechnol.,* 2014, **9**, 927.
8 J. Yan and B. Saunders, *RSC Adv.,* 2014, **4**, 43286.
9 Y. Yang, J. Xiao, H. Wei, L. Zhu, D. Li, Y. Luo, H. Wu and Q. Meng, *RSC Adv.,* 2014, **4**, 52825.
10 L. Etgar, P. Gao, Z. Xue, Q. Peng, A. Chandiran, B. Liu, M. Nazeeruddin and M. Grätzel, *J. Am. Chem. Soc.,* 2012, **134**, 17396.
11 M. Cai, V. Tiong, T. Hreid, J. Bell and H. Wang, *J. Mater. Chem. A,* 2015, **3**, 2784.
12 J. Xiao, J. Shi, H. Liu, Y. Xu, S. Lv, Y. Luo, D. Li, Q. Meng and Y. Li, *Adv. Energy Mater.,* 2015, **5**, 1401943.
13 X. Yin, Y. Guo, Z. Xue, P. Xu, M. He and B. Liu, *Nano. Res.,* 2015, **8**, 1997.
14 T. Liu, Q. Hu, J. Wu, K. Chen, L. Zhao, F. Liu, C. Wang, H. Lu, S. Jia, T. Russell, R. Zhu and Q. Gong, *Adv. Energy Mater.*, 2015, DOI: 10.1002/aenm.201501890.
15 N. Ahn, D. Son, I. Jang, S. Kang, M. Choi and N. Park, *J. Am. Chem. Soc.,* 2015, **137**, 8696.
16 H. Zhou, Q. Chen, G. Li, S. Luo, T. Song, H. Duan, Z. Hong, J. You, Y. Liu and Y. Yang, *Science,* 2014, **345**, 542.
17 J. Lee, D. Seol, A. Cho and N. Park, *Adv. Mater.,* 2014, **26**, 4991.
18 S. Pang, H. Hu, J. Zhang, S. Lv, Y. Yu, F. Wei, T. Qin, H. Xu, Z. Liu and G. Cui, *Chem. Mater.,* 2014, **26**, 1485.
19 F. Wang, H. Xu, H. Xu and N. Zhao, *Adv. Funct. Mater.,* 2015, **25**, 1120.
20 M. Hu, L. Liu, A. Mei, Y. Yang, T. Liu and H. Han, *J. Mater. Chem. A,* 2014, **2**, 17115.
21 D. Seol, J. Lee and N. Park, *ChemSusChem,* 2015, **8**, 2414.
22 G. Eperon, D. Bryant, J. Troughton, S. Stranks, M. Johnston, T. Watson, D. Worsley and H. Snaith, *J. Phys. Chem. Lett.,* 2015, **6**, 129.
23 F. Hanusch, E. Wiesenmayer, E. Mankel, A. Binek, P. Angloher, C. Fraunhofer, N. Giesbrecht, J. Feckl, W. Jaegermann, D. Johrendt, T. Bein and P. Docampo, *J. Phys. Chem. Lett.,* 2014, **5**, 2791.
24 D. Yuan, A. Gorka, M. Xu, Z. Wang and L. Liao, *Phys. Chem. Chem. Phys.,* 2015, **17**, 19745.
25 M. Leyden, M. Lee, S. Raga and Y. Qi, *J. Mater. Chem. A,* 2015, **3**, 16097.
26 S. Aharon, A. Dymshits, A. Rotem and L. Etgar, *J. Mater. Chem. A,* 2015, **3**, 9171.
27 T. Koh, K. Fu, Y. Fang, S. Chen, T. Sum, N. Mathews, S. Mhaisalkar, P. Boix and T. Baikie, *J. Phys. Chem. C,* 2014, **118**, 16458.
28 C. Stoumpos, C. Malliakas and M. Kanatzidis, *Inorg. Chem.,* 2013, **52**, 9019.
29 H. Zhang, J. Shi, J. Dong, X. Xu, Y. Luo, D. Li and Q. Meng, *J. Energy Chem*., 2015, **24**, 707.
30 G. Eperon, S. Stranks, C. Menelaou, M. Johnston, L. Herz and H. Snaith, *Energy Environ. Sci.,* 2014, **7**, 982.
31 N. Pellet, P. Gao, G. Gregori, T. Yang, M. Nazeeruddin, J. Maier and M. Grätzel, *Angew. Chem., Int. Ed.,* 2014, **53**, 3151.
32 N. Jeon, J. Noh, W. Yang, Y. Kim, S. Ryu, J. Seo and S. Seok, *Nature,* 2015, **517**, 476.
33 J. Liu, Y. Shirai, X. Yang, Y. Yue, W. Chen, Y. Wu, A. Islam and L. Han, *Adv. Mater.,* 2015, **27**, 4918.
34 Y. Chen, T. Chen and L. Dai, *Adv. Mater.,* 2015, **27**, 1053.
35 H. Choi, J. Jeong, H. Kim, S. Kim, B. Walker, G. Kim and J. Kim, *Nano Energy,* 2014, **7**, 80.
36 C. Bi, Y. Yuan, Y. Fang and J. Huang, *Adv. Energy Mater.,* 2015, **5**, 1401616.
37 J. Noh, S. Im, J. Heo, T. Mandal and S. Seok, *Nano Lett.,* 2013, **13**, 1764.
38 A. Binek, F. Hanusch, P. Docampo and T. Bein, *J. Phys. Chem. Lett.,* 2015, **6**, 1249.

39 W. Yang, J. Noh, N. Jeon, Y. Kim, S. Ryu, J. Seo and S. Seok, *Science,* 2015, **348**, 1234.
40 L. Protesescu, S. Yakunin, M. Bodnarchuk, F. Krieg, R. Caputo, C. Hendon, R. Yang, A. Walsh and M. Kovalenko, *Nano Lett.,* 2015, **15**, 3692.
41 Q. Akkerman, V. D'Innocenzo, S. Accornero, A. Scarpellini, A. Petrozza, M. Prato and L. Manna, *J. Am. Chem. Soc.,* 2015, **137**, 10276.
42 X. Xia, H. Li, W. Wu, Y. Li, D. Fei, C. Gao and X. Liu, *ACS Appl. Mater. Interfaces,* 2015, **7**, 16907.
43 E. Juarez-Perez, M. Wuβler, F. Fabregat-Santiago, K. Lakus-Wollny, E. Mankel, T. Mayer, W. Jaegermann and I. Mora-Sero, *J. Phys. Chem. Lett.,* 2014, **5**, 680.
44 J. Zhang, E. Juárez-Pérez, I. Mora-Seró, B. Viana and T. Pauporté, *J. Mater. Chem. A,* 2015, **3**, 4909.
45 M. Lv, X. Dong, X. Fang, B. Lin, S. Zhang, X. Xu, J. Ding and N. Yuan, *RSC Adv.,* 2015, **5**, 93957.

Table of contents

High efficiency and humidity stability perovskite solar cells based on $FA_{1-x}Cs_xPbI_3$ solid solution are prepared by spray reaction technology.